Available on CMS information server

CMS NOTE 1997/103

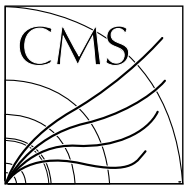

The Compact Muon Solenoid Experiment

CMS Note

Mailing address: CMS CERN, CH-1211 GENEVA 23, Switzerland

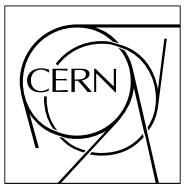

11 December 1997

Test Beam Results on a Double-Sided Microstrip Detector Before and After Neutron Irradiation

M. M. Angarano, D. Creanza, M. de Palma, L. Fiore, G. Maggi, S. My, A. Pompili, G. Raso, P. Tempesta, G. Selvaggi, L. Silvestris[a)]

Dipartimento di Fisica and INFN, Bari, Italy

D. Boemi

Dipartimento di Fisica and INFN, Catania, Italy

Abstract

We present the results of beam tests carried out on an AC-coupled, poly biased, double-sided, double-metal silicon microstrip detector. The detector has been tested in the beam three times: before the neutron irradiation, right after and one year later. After irradiation a decrease in signal-to-noise ratio (S/N) has been observed for both sides. It has been interpreted in terms of noise increase due to higher interstrip capacitance and leakage current. The high efficiency characterizing the device has been preserved after irradiation, and a substantial stability of the performances has been observed after one year, the detector being kept at $0^{\circ}\mathrm{C}$.

[a)] Now at CERN, Geneva, Switzerland

1 Introduction

The silicon detectors used in the tracking system of the CMS experiment at LHC will be exposed to very high radiation fluences. With time they will undergo type inversion and will require higher bias voltage values to be fully depleted. The leakage current will significantly increase, while changes in the interface properties due to radiation will increase the interstrip capacitance. These facts lead to an increase of noise. Usually, in order to avoid anti-annealing processes and keep noise and thermal effects due to leakage current whithin acceptable levels, heavily irradiated detectors must be operated at low temperature. Since the performances of the silicon microstrip detectors strongly depend on signal-to-noise ratio, careful tests with particle beams in realistic operating conditions are necessary. The aim of this study is to investigate the performance of a double-sided ($p^+ - n - n^+$), double-metal microstrip detector irradiated at doses beyond type inversion and operated at temperatures ranging between $0°\mathrm{C}$ and $-10°\mathrm{C}$.

2 Detector characteristics and irradiation conditions

For this study we have used a double-sided, double-metal (DSDM) silicon microstrip detector produced by Hamamatsu Photonics [1]. The active area is $5.45 \times 3.2\, cm^2$. The detector features integrated coupling capacitors and polysilicon bias resistors on both sides. The isolation of the n^+ strips on the ohmic side is achieved by p^+ blocking strips. The main characteristics of the device are summarized in table 1. The read-out pitch is $50\ \mu m$ on the p-side, leaving one floating strip in between two read-out strips, and $84\ \mu m$ on the n-side, since two adjacent strips are shortened and read-out together.

Table 1: Detector design parameters

$parameter$	$p-side$	$n-side$
physical strip pitch	$25\ \mu m$	$42\ \mu m$
read-out strip pitch	$50\ \mu m$	$84\ \mu m$
strip length	$5.45\ cm$	$3.2\ cm$
implant width	$12\ \mu m$	$14\ \mu m$
number of strips	1281	1280
detector thickness	$300\ \mu m$	

The most relevant electrical parameters of the device are summarized in table 2.

Table 2: Detector electrical parameters

$parameter$	$p-side$	$n-side$
Leakage current per strip: $I_{leak/str}$ $[nA]$ $(at\ 20°\mathrm{C})$	0.8	1.6
Polysilicon bias resistor: R_b $[M\Omega]$	> 10	> 20
Strip resistance: R_s $[\Omega]$	35	15
Coupling capacitance: C_{ac} $[pF/cm]$	20	40
Bulk capacitance: C_b $[pF/cm]$	$\simeq .1$	$\simeq .1$
Interstrip capacitance: C_1 $[pF/cm]$	$\simeq .65$	$\simeq 1.5$
2^{nd} neighbour strip capacitance: C_2 $[pF/cm]$	$\simeq .065$	$\simeq .15$
C_{str} $[pF]$	$\simeq 5.19$	$\simeq 11.2$
$C_{tot} = C_{str} \cdot C_{ac} / (C_{ac} + C_{str})$ $[pF]$	$\simeq 4.75$	$\simeq 10.3$

Except for leakage current, the electrical parameters in table 2 are given by Hamamatsu or can be found in the references [4, 5, 6, 7]. Moreover, the values for the quantities referred to the n-side are listed taking into account that two adjacent strips are shortened and read-out together. The capacitance C_2 has been assumed to be $\simeq 10\%$ of C_1. The capacitance C_{str} has been calculated, considering the read-out configurations and according to the following formulas [8]: on the p-side $C_{str} = C_b + 2 \cdot (C_1' + C_2)$, where $C_1' = C_1 \cdot (C_b + C_1 + C_2) / (C_b + 2C_1 + C_2)$; on the n-side $C_{str} = 2C_b + 2 \cdot (C_1 + C_2)$.

The device was irradiated (at room temperature and without bias) with 1 MeV neutrons at CERN PSAIF facility [2], up to a fluence of $3.1 \times 10^{13} n\, cm^{-2}$, reaching type inversion, as expected from the estimated inversion fluence $\Phi_{inv} = 1.1 \times 10^{13} cm^{-2}$. After irradiation the detector has been kept at $\simeq 0°\mathrm{C}$ in order to inhibit both annealing and anti-annealing effects.

In fig. 1 the total detector leakage current versus bias voltage (V_{bias}), measured before and after irradiation, is shown. The depletion voltage is around $40V$ both before and after irradiation, in agreement with the estimated value for the actual irradiation dose.

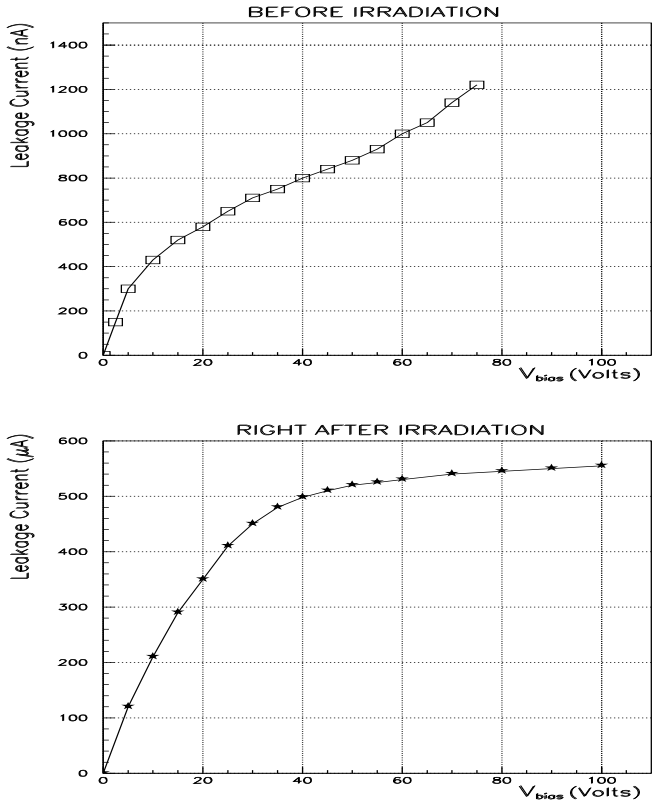

Figure 1: Detector total leakage current before and after irradiation.

The increase of the leakage current at full depletion is $\simeq \ 500\mu A$, which implies a current damage constant $\alpha = 3.1 \times 10^{-17} Acm^{-1}$, within the expected range [3].

The inverse leakage current per strip after irradiation, at $-5^{\circ}\mathrm{C}$ was $40nA$ on p-side and $80nA$ on n-side. In the S/N estimation after irradiation it has been assumed a total capacitance increase of 50% on the p-side [9] and of 20% on the n-side [6, 7].

3 Experimental set up and data analysis

The detector was glued on a properly machined G-10 frame, housing the read-out electronics: an array of Pre-Mux128 preamplifiers [10], set to a shaping time of $45\ ns$.

The detector was tested in a particle beam at three subsequent times: before irradiation (July '96), soon after the irradiation (September '96) and one year later. In between the data-taking periods after the irradiation the device was permanently kept at $\simeq 0^{\circ}\mathrm{C}$. A $20\,GeV$ pions beam, available at the X7 CERN area, was used in July and September 1996, whereas a $100\,GeV$ muons beam was used at the X5 CERN area in August 1997. Data were taken at room temperature for the unirradiated detector and at $-10^{\circ}\mathrm{C}$,$-5^{\circ}\mathrm{C}$, $0^{\circ}\mathrm{C}$ for the irradiated one. For low temperature runs, the frame housing the detector and the electronics was mounted inside a thermally insulated box in which cooled air was circulated. The temperature was monitored inside the box and resulted to be stable within $\pm 0.5^{\circ}\mathrm{C}$. The detector was biased through the n-side, and the related electronics was operated with V_{bias} as reference voltage. A decoupling circuit, based on opto-electronic components, was used to refer the output signal for the n-side to the common ground level.

On the beam line, the detector was placed in between two pairs of double-sided silicon planes within the "Bari telescope" [11]. In the last beam test period a read-out electronics failure didn't allow data taking for the p-side.

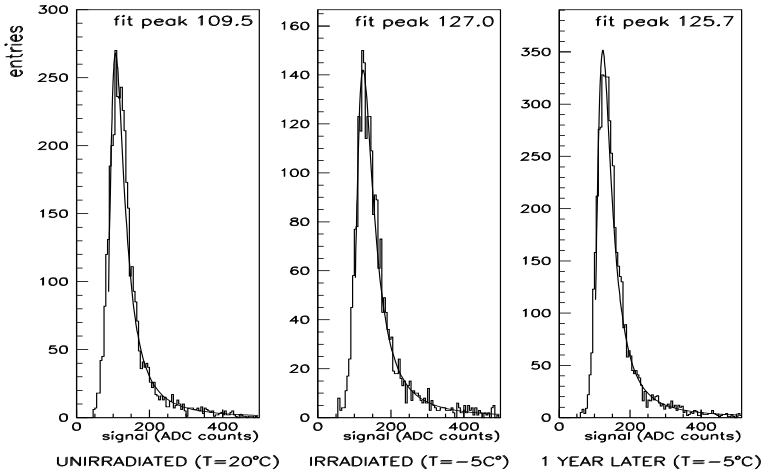

Figure 2: n-side cluster signal distributions with superimposed Landau fits ($V_{bias} = 60V$).

Data analysis has been performed using a software package developed by the CMS collaboration. This package allows the signal extraction by pedestal and common mode subtraction and the cluster reconstruction on an event-by-event basis, using an algorithm described in [12]. This algorithm requires a set of constants and thresholds to be defined by optimization studies. The most important parameters used in this analysis are summarized in table 3.

Table 3: Cluster reconstruction cuts

Seed strip S/N	3
Neighbour strips S/N	2
Cluster S/N	5
Cluster maximal extension	14
Max dead strips per cluster	1

4 Results

The detector performances have been tested by studying signal charge correlation, S/N and efficiency for both sides, for different values of detector bias voltage and operating temperature.

4.1 Cluster signal-to-noise ratio

A careful study of the detector noise for each channel has been performed before and after irradiation. Obviously after irradiation we measure higher noise, but no additional dead or noisy channel has been observed. Fig. 2 shows the n-side cluster signal distributions relative to the three different data-taking periods, at the same bias voltage. It is worth noticing that the Landau shape is well preserved before and after irradiation. The peak value for the irradiated device doesn't change after 1 year, while the difference of the most probable signal before and after irradiation (109.5 vs 127 ADC counts) is attributed to the different operating temperature.

This effect has been studied in detail in figg. 3 and 4 which show the cluster signal as a function of V_{bias}. Systematically the cluster signal for the irradiated detector (operated at $-5^{\circ}\mathrm{C}$) is 10% higher than the corresponding value for the unirradiated device (operated at $20^{\circ}\mathrm{C}$). This behaviour is explained by the decrease with temperature of the recombination rate, which increases the charge collection efficiency [12].

The correlation between cluster signals on the two sides is very good both before and after irradiation, as shown in fig. 5. The amount of charge on the n-side is slightly lower with respect to the p-side. This can be mainly ascribed to losses and attenuations in decoupling the read-out line from the high voltage circuitry. An effort to improve the filtering scheme is under way.

The cluster noise of the irradiated detector is well described by gaussian distributions without significant tails (fig. 6). Figures 7 and 8 show the cluster noise N as a function of V_{bias} for both sides of the device before and after

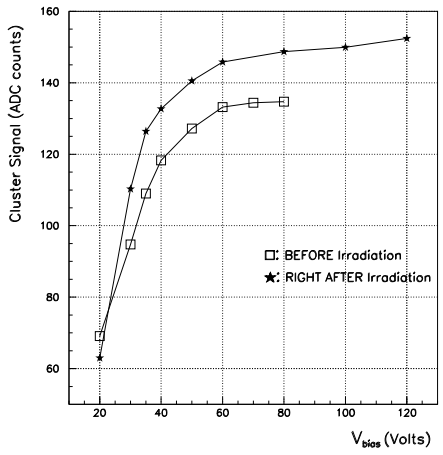

Figure 3: p-side cluster signal as a function of V_{bias}.

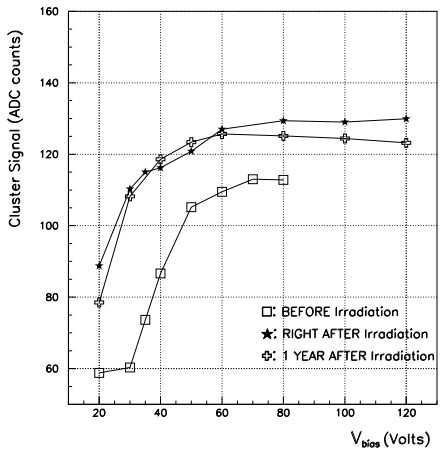

Figure 4: n-side cluster signal as a function of V_{bias}.

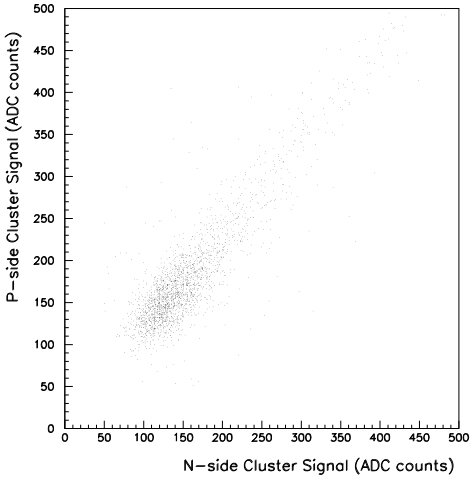

Figure 5: Cluster signal correlation right after irradiation ($V_{bias} = 60V$).

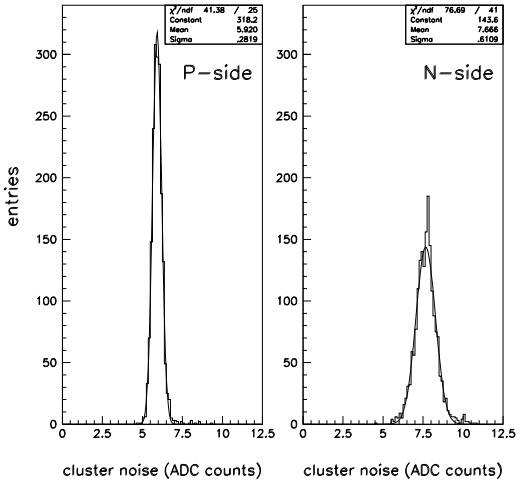

Figure 6: Cluster noise distributions with superimposed gaussian fits right after irradiation ($V_{bias} = 80V$).

irradiation. For a fully depleted detector the noise is higher after irradiation on both sides due to the increase of the interstrip capacitance and of the leakage current. Typical values in ADC counts are: $N \simeq 4$ before and $\simeq 6$ after irradiation for the p-side, whereas 6.2 and 7.6 are the corresponding values for the n-side.

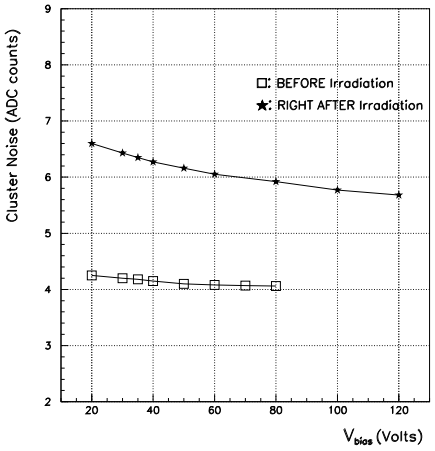

Figure 7: p-side cluster noise as a function of V_{bias}.

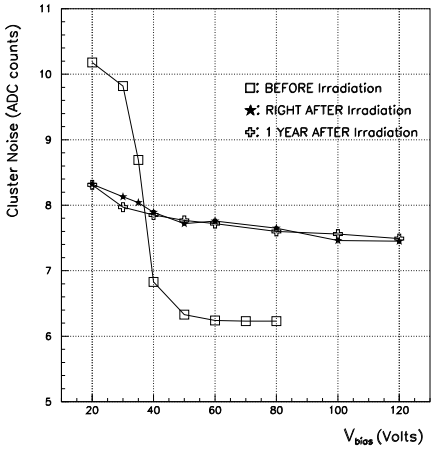

Figure 8: n-side cluster noise as a function of V_{bias}.

The cluster S/N ratio is defined as the ratio between the peak value of the Landau signal distribution and the gaussian fit to the cluster noise distribution. In figg. 9 and 10 the S/N ratio as a function of V_{bias} is presented, before and after irradiation, for both sides. The S/N ratio decreases by 5% on the n-side and by 20% on the p-side. Typical values at full depletion are summarized in table 4.

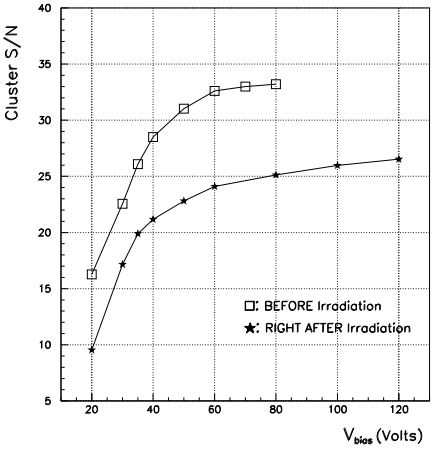

Figure 9: p-side cluster S/N as a function of V_{bias}.

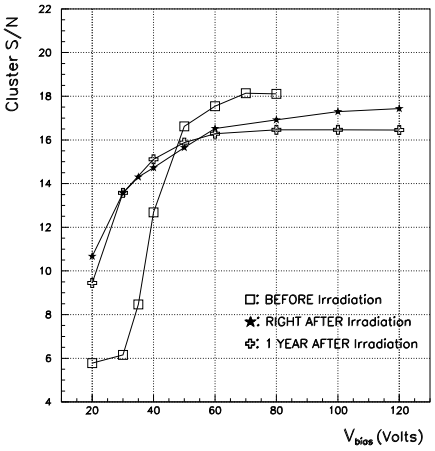

Figure 10: n-side cluster S/N as a function of V_{bias}.

The S/N ratio can be evaluated from the expected signal and the calculated noise [7] according to the scheme presented in table 4, where the estimated values for the different factors contributing to the noise are explicitly listed. A good agreement can be obtained between estimated and measured values of S/N for the p-side by assuming a 50% increase of the detector capacitance with irradiation. The discrepancy for the n-side is attributed to the above mentioned read-out filtering problem and partly to the additional capacitance introduced by the second metal layer, as already noticed in [13].

Both before and after irradiation the dominant contribution to the noise comes from the detector total input capacitance (see table 4). Fig. 10 shows the stability of the S/N after one year, with the detector permanently kept

Table 4: Detector electrical parameters

quantities expressed in e^- (except S/N)	$p-side$		$n-side$	
	$before$	$after$	$before$	$after$
$ENC_{el} \simeq 500 + 38 \cdot C_{tot}\,[pF]/pF$	680	770	890	970
$ENC_{sr} \simeq 24 \cdot C_{tot}[pF] \cdot \sqrt{R_s[\Omega]/t_p[ns]}$	100	150	145	170
$ENC_{br} \simeq 24 \cdot \sqrt{t_p[ns]/R_b[M\Omega]}$	50	50	35	35
$ENC_{leak} \simeq 108 \cdot \sqrt{I_{leak/str}[\mu A] \cdot t_p[ns]}$	20	145	30	205
ENC_{tot}	690	800	905	1005
MIP's released charge (S)	24000	24000	24000	24000
Collected charge $S' = S \cdot C_{ac}/(C_{ac} + C_{str})$	22910	21096	22070	21670
Calculated S/N: S'/ENC_{tot}	33.2	26.4	24.4	21.6
Measured S/N	33	26	18	17

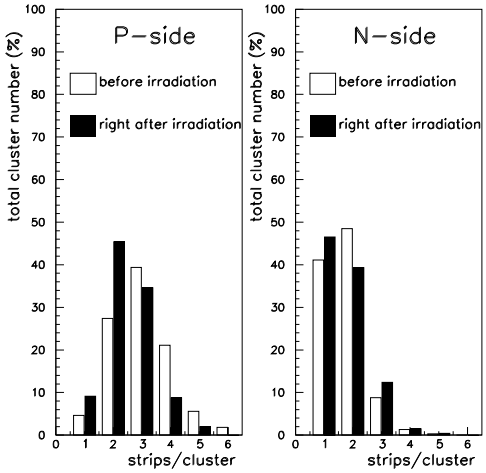

Figure 11: Distribution of the number of strips per cluster at $V_{bias} = 80V$.

around $0°\mathrm{C}$ in order to inhibit annealing and reverse annealing processes.

4.2 Inversion effects

It is worth noticing the different behaviour of the two sides before and after the effective type inversion induced by the irradiation. Before inversion the depletion region extends from the p-side and for $V_{bias} < V_{depletion}$ the n^+ strips are shortened, the noise is huge and the S/N marginal. At $V_{bias} \simeq V_{depletion}$ the n^+ strips are isolated and a sharp rise of the S/N is visible (figg. 8, 10). The situation is not really symmetric after the inversion. Now the depletion region starts from the n-side, but even when the device is not fully depleted the p^+ strips are still isolated since the inversion of the bulk does not imply the inversion of the surface states which dominate the interface charge and the interstrip impedance. As a result, the noise of the p-side after inversion is higher for the increase of interstrip capacitance but still manageable and the signal-to-noise ratio shows a smooth and progressive increase with bias reflecting the increase in signal due to an extended depleted region and the reduction of noise due to the effect of V_{bias} on the interstrip capacitance (figg. 7, 9).

4.3 Charge division mechanism

For perpendicular tracks and no magnetic field the cluster size depends on the read-out pitch, the strip width, the mechanism of diffusion and the clustering algorythm. Fig. 11 shows, for both sides and for $V_{bias} = 80V$, the distribution of the number of strips per cluster before and after irradiation.

Figg. 12 and 13 show the average cluster width as a function of V_{bias}. The average number of strips per cluster is lower for the irradiated detector: 10% decrease of the cluster width is expected from the change of the operating temperature from $20°\mathrm{C}$ to $-5°\mathrm{C}$ [12]; at lower temperature, in fact, recombination mechanism is less probable, charge collection is faster and diffusion effects are relatively less important.

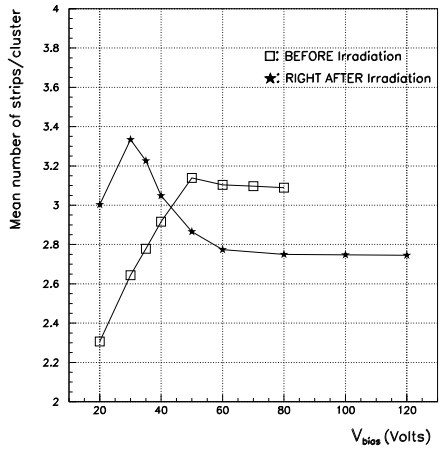

Figure 12: p-side cluster width as a function of V_{bias}.

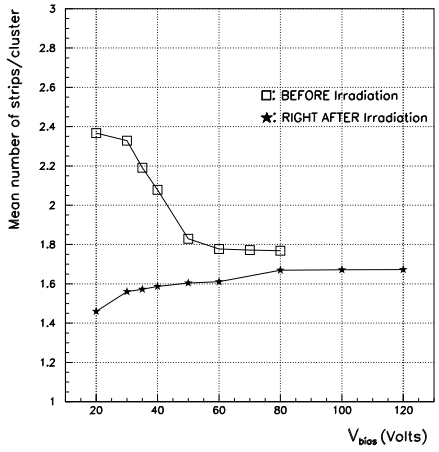

Figure 13: n-side cluster width as a function of V_{bias}.

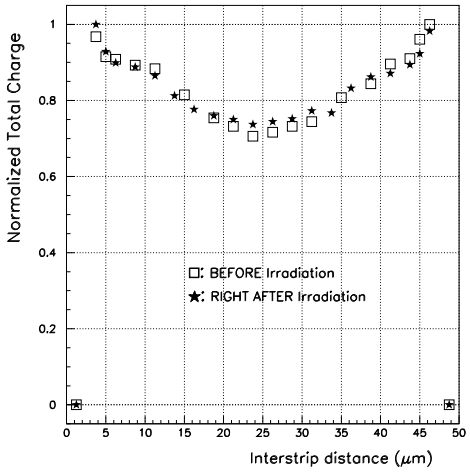

Figure 14: Normalized total charge as a function of V_{bias}.

When floating strips are left between two read-out electrodes, some capacitive charge loss towards the back-plane is expected. For the p-side we have studied the effect of a read-out pitch of $50\mu m$ with one strip left floating in between. Tracks reconstructed by the telescope are extrapolated to the detector under study and for each impact point the charge collected by the two read-out electrodes is recorded. The study was limited to 2-strips clusters. In order to guarantee a more precise reconstruction, only events for which the difference between extrapolated and measured impact point is within 1σ of the relative distribution have been chosen. The normalized interstrip total charge distributions before and after irradiation are compared in fig. 14. In the region of the floating strip a charge collection efficiency of 75% is observed; the 25% loss is substantially unaffected by irradiation.

4.4 Efficiency

The hit efficiency has been determined with the following criteria: a) first we have selected a detector region free of noisy channels and in which the beam profile is uniform; b) for every track reconstructed by the telescope, a $150\ \mu m$ window centered on the extrapolated impact point on the detector has been considered. c) Then we have looked for a cluster associated to the track. d) Efficiency is defined as the ratio between measured and expected number of clusters. Figg. 15 and 16 show the efficiencies as a function of V_{bias}, before and after irradiation, for both sides. In the latter the efficiency measured 1 year after the irradiation is also presented. The high efficiency ($> 98\%$ for p-side and $\simeq 97\%$ for n-side) observed for the unirradiated detector in the plateau region can be

essentially reproduced for both sides soon after the irradiation and one year later.

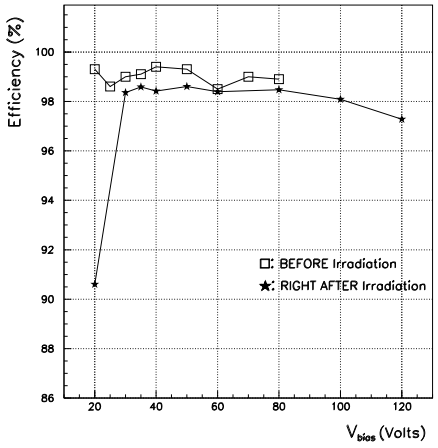

Figure 15: p-side efficiency as a function of V_{bias}.

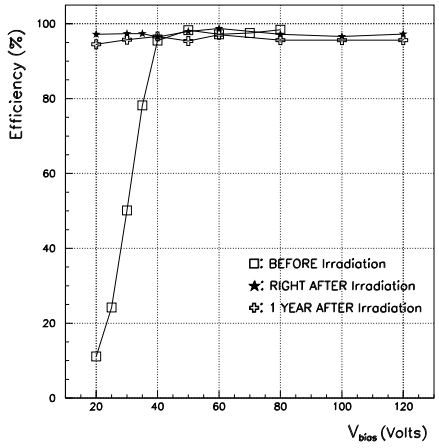

Figure 16: n-side efficiency as a function of V_{bias}.

4.5 Temperature effects

A study of the temperature effects on S, N and S/N for the irradiated device has been also performed. Data were taken at three different temperatures: 0°C, -5°C and -10°C. In figures 17, 18 the signal S as a function of V_{bias} at these three temperatures is presented for both sides. The collected charge increases with decreasing the temperature.

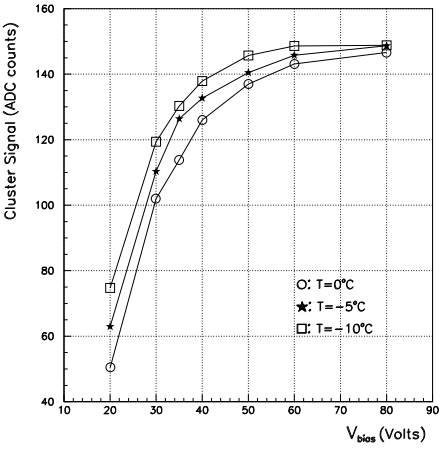

Figure 17: Cluster signal on the p-side as a function of V_{bias}, right after irradiation

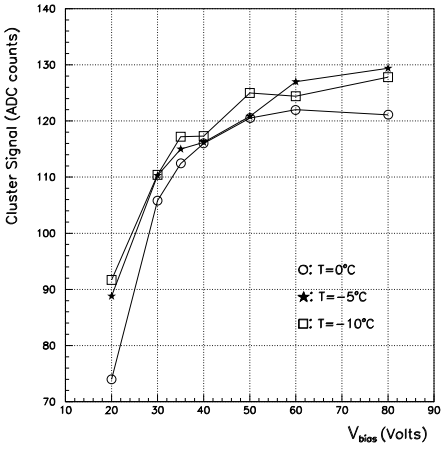

Figure 18: Cluster signal on the n-side as a function of V_{bias}, right after irradiation

In figures 19, 20 the noise N as a function of V_{bias} for different temperatures is presented for both sides. There is an opposite behaviour for the two sides: with decreasing the temperature N decreases on the n-side but increases on the p-side. In spite of this behaviour the S/N increases with decreasing the temperature on both sides (see figures 21, 22).

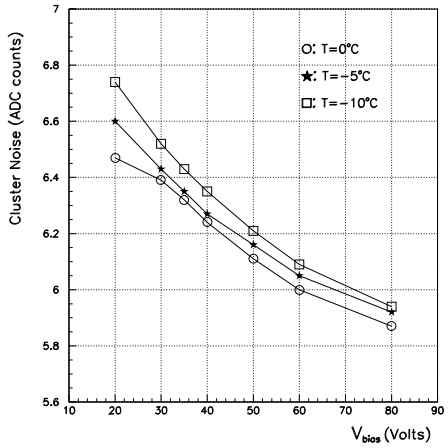

Figure 19: Cluster noise on the p-side as a function of V_{bias}, right after irradiation

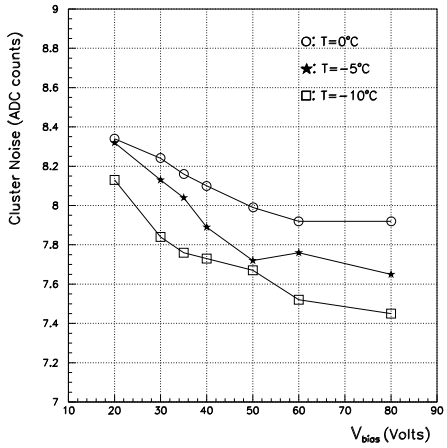

Figure 20: Cluster noise on the n-side as a function of V_{bias}, right after irradiation

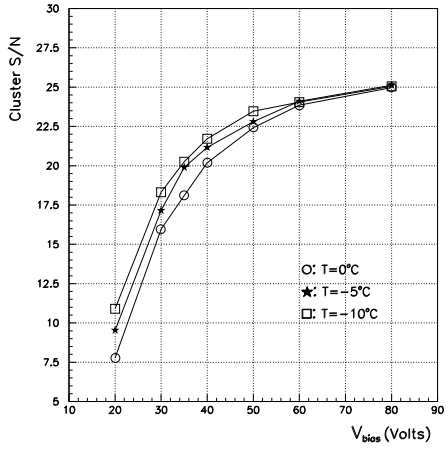

Figure 21: Cluster S/N on p-side as a function of V_{bias}, right after irradiation

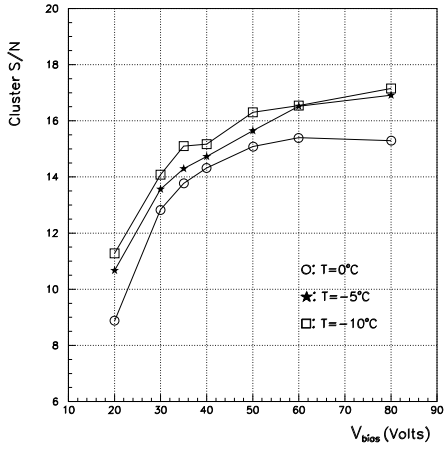

Figure 22: Cluster S/N on n-side as a function of V_{bias}, right after irradiation

5 Conclusions:

A DSDM silicon microstrip detector produced by Hamamatsu Photonics, irradiated up to an equivalent fluence of $3.1 \times 10^{13}\, n\, cm^{-2}$, beyond type inversion, has been tested. Signal, noise, S/N ratio and efficiency, as a function of the bias voltage and the operating temperature, have been studied before, right after and 1 year after irradiation (the detector being kept around $0^{\circ}\mathrm{C}$). The double metal technology and the ohmic side isolation by p^{+} blocking strips worked satisfactorily also after type inversion. No appreciable increase in the number of dead or noisy channels have been noticed after irradiation. A S/N reduction on both sides, after irradiation has been observed. This can be explained with the higher noise expected for an increased interstrip capacitance and a higher leakage current. The high efficiency characterizing the device has been found to be substantially unaffected by radiation. From charge division and collection studies no appreciable different behaviour has been observed after irradiation. The substantial stability of S/N and efficiency performances one year after irradiation confirms that keeping the detector continuously around $0^{\circ}\mathrm{C}$ allows for a safe long term operation of irradiated devices.

References

[1] Hamamatsu Photonics Co., Hamamatsu 435, Japan.

[2] PSAIF, PS-ACOL neutron facility, CERN-HS-CFM/IR/91-10.

[3] G. N. Taylor et al., N.I.M. A383 (1996) 144-154.

[4] V. Chabaud et al., N.I.M. A368 (1996) 314-332.

[5] C. Troncon, Nuclear Physics B, Proc. Suppl. 44 (1995) 287-291.

[6] E. Barberis et al., *Analysis of Capacitance Measurements on Silicon Microstrip Detectors*, SCIPP 93/39.

[7] T. Oshugi et al., N.I.M. A342 (1994) 16-21.

[8] C. Bozzi, *Signal-to-Noise Evaluations for the CMS Silicon Microstrip Detectors*, CMS NOTE 1997/026.

[9] M. Krammer, *Estimation of S/N in the CMS Si-tracker*, CMS Internal Report, 22/10/97.

[10] L. L. Jones, *PreMux128 Specification*, version 2.3, 1995.

[11] L. Celano et al., N.I.M. A381 (1996) 49-56.

[12] P. Coyle et al., *Test beam results from prototypes of the upgraded Aleph vertex detector*, ALEPH Note 94-069.

[13] O. Adriani et al., N.I.M. A396 (1997) 76-92.